Title
Structure and Thermodynamics of Hybrid Organic–Inorganic Diblock Copolymers with Salt

Journal
Macromolecules, 52(9)

ISSN
0024-9297

Authors
Sethi, Gurmukh K
Jung, Ha Young
Loo, Whitney S
et al.

Publication Date
2019-05-14

DOI
10.1021/acs.macromol.9b00042

Peer reviewed

Structure and thermodynamics of hybrid organic-inorganic diblock copolymers with salt

Gurmukh K. Sethi[†,‡], Ha Young Jung[#], Whitney S. Loo[‖], Simar Sawhney[‖], Moon Jeong Park[#], Nitash P. Balsara[‖,‡,§,⊥,], and Irune Villaluenga[§,*]*

[†]Department of Materials Science and Engineering and [‖]Department of Chemical and Biomolecular Engineering, University of California, Berkeley, California 94720, USA

[#]Department of Chemistry, Pohang University of Science and Technology (POSTECH), Pohang, 790-784 Korea

[‡]Materials Science Division, [§]Joint Center for Energy Storage Research (JCESR), and [⊥]Energy Storage and Distributed Resources Division, Lawrence Berkeley National Laboratory, Berkeley, California 94720, USA

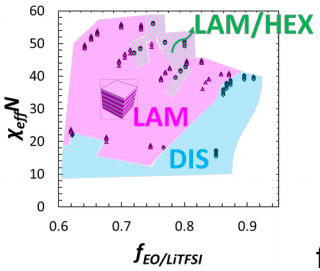

for Table of Contents use only

ABSTRACT**.** We examine the phase behavior of a hybrid organic-inorganic diblock copolymer/salt mixtures. The experimental system comprises

poly(ethylene oxide)-*block*-polyhedral oligomeric silsesquioxane (PEO-POSS) mixed with a lithium bis(trifluoromethanesulfonyl) imide (LiTFSI) salt. While the diblock copolymers without salt exhibit classical order-to-disorder transition behavior with increasing temperature, the PEO-POSS/salt mixtures exhibit disorder-to-order transitions with increasing temperature. Analysis of small angle x-ray scattering data from the disordered state using Leibler's Random Phase Approximation enables the determination of an effective Flory-Huggins interaction parameter, χ_{eff}, for the electrolytes. Unlike conventional systems, χ_{eff} increases with increasing temperature. A simple expression is proposed to describe the dependence of χ_{eff} on temperature and salt concentration. This enables calculation of the segregation strength, $\chi_{eff}N$, for both ordered and disordered electrolytes. The composition of the electrolytes is quantified by $f_{EO/LiTFSI}$, the volume fraction of the salt-containing poly(ethylene oxide)-rich phase. The morphology of electrolytes is presented on a $\chi_{eff}N$ versus $f_{EO/LiTFSI}$ phase diagram. Over the values of $f_{EO/LiTFSI}$ studied (0.61-0.91) only two ordered phases were found: lamellae and coexisting lamellae/hexagonally packed cylinders.

INTRODUCTION**.** Solid polymer electrolytes are more electrochemically and thermally stable in comparison to conventional liquid electrolytes for lithium batteries[1]. Linear block copolymers, wherein two chemically distinct polymer chains are chemically bonded together, can provide separate ion-conduction channels as well as mechanically rigid, non-conducting channels. The classic

balance between entropy and enthalpy in addition to covalent bonds between the two blocks causes these materials to self-assemble into nanostructured morphologies with length scales on the order of tens of nanometers. The thermodynamics of all organic electrolytes with salt has been extensively studied in experimental[2-12] and theoretical systems.[13-15] Though there have been studies conducted on the electrochemical properties,[16–20] mechanical properties,[21,22] and ordered phases of hybrid inorganic-organic copolymers,[23-34] the thermodynamic behavior of inorganic-organic copolymers containing salt has yet to be systematically studied.

Here, we present the morphology using small angle x-ray scattering and TEM of poly(ethylene oxide)-*block*-polyhedral oligomeric silsesquioxane (PEO-POSS) mixed with a lithium bis(trifluoromethanesulfonyl) imide (LiTFSI) salt. Each POSS moiety is inorganic silica-like core surrounded by a shell of organic butyl groups and is about 10 times larger than most typical monomers with molecular weight close to 1000 g mol^{-1}.[35] This bulkiness of POSS gives rise to unusual physical properties due to a high degree of conformational asymmetry and relative stiffness in comparison to PEO. PEO-POSS is considered a rod-coil type diblock copolymer: the chain behaves as a rigid rod for length corresponding to number of POSS monomers whereas the longer chain portions follow ideal gaussian statistics.[36-44]

The thermodynamic data from 24 PEO-POSS/LiTFSI mixtures are presented on a universal phase diagram. We use a simple equation to quantify the temperature dependence of the interaction parameter for

copolymers with salt concentration ranging from $0.02 \leq r \leq 0.30$ and volume fraction of the PEO/LiTFSI rich phase, $f_{EO/LiTFSI}$, between 0.61 to 0.91. The present paper builds upon work published in a letter wherein the morphology of electrolytes obtained from one PEO-POSS copolymer was described.[45]

EXPERIMENTAL

Materials. PEO-acrylate (M_w = 5 kg/mol), anhydrous ethanol, anhydrous xylene, diethyl ether and tetrahydrofuran (THF) were purchased from Sigma-Aldrich, acryloisobutyl polyhedral oligomeric silsesquioxane (POSS) was purchased from Hybrid Plastic, BlocBuilder MA was kindly provided by Arkema, and lithium bis(trifluoromethanesulfonyl)-imide, $Li[N(SO_2CF_3)_2]$ (LiTFSI), was purchased from Novolyte. All chemicals were used as received.

Synthesis. PEO-POSS block copolymer was synthesized by nitroxide-mediated radical polymerization (NMP). First, PEO-acrylate was reacted with BlocBuilder MA in anhydrous ethanol at 100 ºC under argon for 4h. PEO-based macroalkoxyamine was collected by precipitation in cold diethylether. Then, the POSS-acryloisobutyl monomer was polymerized using the PEO-based macroalkoxyamine as initiator in anhydrous xylene at 115 °C for 24h. The product was isolated by precipitation in cold diethyl ether, and then, centrifugation at 6500 rpm for 15 min. This step was repeated three times to obtain a white solid powder. Molecular weight was determined using H-NMR spectroscopy. The polymers used in this study are called PEO-POSS(x-y)

where x and y are the molecular weights of the PEO, M_{PEO}, and POSS, M_{PPOSS}, blocks in kg mol^{-1} respectively. PEO-POSS structure is shown in Figure 1. The overall degree of polymerization of each block was calculated by

$$N_i = \frac{M_i}{\rho_i N v_{ref}} [1]$$

where N is the average number of units of each block calculated from the molecular weight of the block without correcting for end groups and v_{ref} is fixed at 0.1 nm^3. The overall degree of polymerization was calculated by

$$N = N_{PEO} + N_{POSS}. [2]$$

A list of the polymer characteristics including the polydispersity index of the block copolymer, Đ, can be found in Table 1.

^{1}H-NMR. The composition of the organic-inorganic copolymers was determined using ^{1}H NMR ($CDCl_3$, Bruker AV400) measurements by integrating the characteristic peaks of the ethylene protons of PEO block (a) at 3.7 ppm versus the isobutyl end protons (b,c) at 0.63-0.65 of the POSS block. ^{1}H NMR profiles are shown in the Supporting Information (Figure S4).

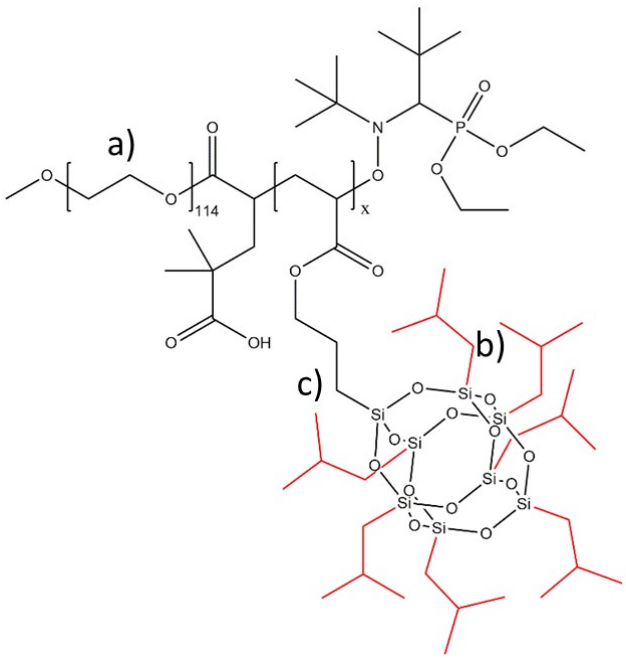

Figure 1. PEO-POSS chemical structure.

Electrolyte Preparation. Electrolytes were prepared by mixing each polymer with LiTFSI. Due to the hygroscopic nature of LiTFSI, all sample preparation was carried out in an argon glovebox (MBraun) where H_2O and O_2 levels were maintained below 0.6 ppm and 1 ppm respectively. PEO-POSS polymer was dried at 90 °C under vacuum in the glovebox antechamber for 48 h, and then transferred into the glovebox. Dry polymer and LiTFSI salt were dissolved into anhydrous THF and the solutions were mixed at 60 °C for a minimum of 12 h. Once the solutes were fully dissolved, the caps were removed from the vials allowing THF to evaporate and leave behind a homogeneous polymer/salt mixture. After drying on a hotplate at 90 °C for 48 h, the electrolytes were transferred to the glovebox antechamber and dried under vacuum for 48 h at 90 °C to remove all of the THF. The dry

electrolytes color ranged from clear to pale yellow and had a waxy consistency at room temperature.

The salt concentration in our copolymer was quantified by r, the molar ratio of lithium ions to ethylene oxide (EO) moieties. We assume that the salt resides exclusively in the PEO domain and determine the volume fraction of the PEO/LiTFSI microphase, $f_{EO/LiTFSI}$, and the volume fraction of the POSS microphase, f_{POSS}, by

$$f_{EO/LiTFSI}(r)=\frac{\nu_{EO}+r\,\nu_{LiTFSI}}{\nu_{EO}+r\,\nu_{LiTFSI}+\frac{M_{PPOSS}M_{EO}}{M_{POSS}M_{PEO}}\nu_{POSS}} [3]$$

$$f_{POSS}(r)=1-f_{EO/LiTFSI}(r). [4]$$

M_{POSS} and M_{EO} are the molar mass of POSS (929.61 g mol^{-1}) and EO monomer units (44.05 g mol^{-1}) respectively; v_{EO}, v_{POSS}, and v_{LiTFSI} are the molar volumes of ethylene oxide monomer units, POSS monomer units and LiTFSI respectively calculated using the following equation

$$\nu_i=\frac{M_i}{\rho_i} [5]$$

where $M_i \wedge \rho_i$ are the molar masses of unit i and density of unit I, respectively. ρ_{LiTFSI} = 2.392 g cm^{-3}; M_{LiTFSI} = 287.09 g mol^{-1};[46] ρ_{PEO} = 1.128 g cm^{-3} and ρ_{POSS}

= 1.30 g cm^{-3} at 90 °C determined by the procedure outlined in ref [45] measuring the weight of a known amount of diblock copolymer. We note that the value of ρ_{POSS} = 1.30 g cm^{-3} holds for polymerized POSS, as in the three diblock copolymers PEO-POSS(5-2), (5-3) and (5-4).

PEO-POSS(5-1) which contains one POSS monomer unit, density was determined through the following experimental method. Samples were heated to 90 °C, weighed, and filled into pre-weighed aluminum pans with a known volume of 0.04 mL. Pans were hermetically sealed in an argon glovebox and excess POSS was carefully cleaned from the pan. The final weight was recorded. Density of the POSS diblock copolymer was determined by dividing the mass by the known volume of sample pans. Measurements were repeated three times to obtain a standard deviation. Density obtained was 1.11 ± 0.08 g mL^{-1}.The range of volume fractions used in this study can be found in Table 1.

Table 1. Characteristics of Polymers

PEO-POSS	POSS units	M_{PEO} (kg mol^{-1})	M_{POSS} (kg mol^{-1})	f_{EO} 90 °C	$f_{EO/LiTFSI}$ r = 0.30	N	$Đ$
(5-1)	1	5	0.9	0.84	0.91	88	1.17
(5-2)	2	5	1.9	0.76	0.86	97	1.06
(5-3)	3	5	2.8	0.67	0.80	109	1.04
(5-4)	4	5	3.7	0.61	0.75	121	1.04

M_{PEO} = molecular weight of the PEO block; M_{POSS} = molecular weight of the POSS block determined by H-NMR; Đ = dispersity; f_{EO} = volume fraction of PEO block at 90 °C; $f_{EO/LiTFSI}$ = volume fraction of PEO block at 90 °C at r = 0.30; N = chain length calculated at 90 °C and using a monomer reference volume of 0.1 nm^{-1}

Differential Scanning Calorimetry. Samples were hermetically sealed in aluminum pans in an argon glovebox. Differential scanning calorimetry (DSC) experiments were run with two heating and cooling cycles with 10 °C min^{-1} heating rates and 2 °C min^{-1} cooling rates using a Thermal Advantage Q200

calorimeter at the Molecular Foundry, LBNL. The temperature ranged from −90 to 130 °C. Melting and glass transition temperatures were obtained from analysis of the second heating stage. DSC curves are shown in the Supporting Information (Figure S1).

Thermogravimetric Analysis. The polymer thermal degradation temperature was determined via thermogravimetric analysis (TGA) using TA Instruments Q5500 TGA-MS at the Molecular Foundry, LBNL. The sample was heated at 10 °C min^{-1} to 300-500 °C under argon. The thermal degradation temperature was recorded at 5 percent reduction in weight of the polymer sample. TGA curves and analysis are shown in the Supporting Information (Figure S3).

Gel Permeation Chromatography. PEO-POSS was characterized by a Malvern Viscotek TDAmax system gel permeation chromatography (GPC) system with a mobile phase of Chloroform using an injection volume of 100 µL and polymer concentration 2.0 g L^{-1}. GPC traces of PEO-POSS in relation to PEO-acrylate confirm the polymerization of the POSS block. Due to the complex molecular structure of the PEO-POSS copolymer and potential interactions between the polymer segments and the columns, we only use the GPC data to confirm addition of POSS segments onto the PEO chain. GPC curves are shown in the Supporting Information (Figure S2).

Small Angle X-ray Scattering. The morphologies of the electrolytes were determined by small-angle x-ray scattering (SAXS). Samples were prepared by pressing the polymer at 90 °C into 1 mm thick rubber spacers with a 1/8 in. inner-diameter and sealed with Kapton windows in custom-designed airtight holders. The samples were annealed at 110 °C under vacuum for at least 48 h. Measurements were performed at beamline 7.3.3. at the Advanced Light Source (ALS) at Lawrence Berkeley National Laboratory and beamline 1–5 at the Stanford Synchrotron Radiation Lightsource (SSRL) at SLAC National Accelerator Laboratory. Samples were mounted in a custom-built heating stage and held at each temperature for at least 30 min before taking measurements. Silver behenate was used to determine the beam center and sample-to-detector distance. The scattered intensity was corrected for beam transmission. Two-dimensional scattering patterns were integrated azimuthally using the Nika program for IGOR Pro[47] to produce one-dimensional scattering profiles and are reported as scattering intensity, I, as a function of the magnitude of the scattering vector, q; $q = 4\pi sin\theta/2\lambda$ where θ is the scattering angle, and λ is the wavelength of the x-rays equal to 1.2398 Å. The samples were heated from room temperature to the highest temperature ranging between 132 to 143 °C in 20 °C increments and cooled in 5-10 °C increments to ensure thermo-reversibility in all phase transitions.

Transmission Electron Microscopy. PEO-POSS electrolytes were hermetically sealed within Showa-Denko pouch material in an argon

glovebox to remain air and moisture free and heated to the desired temperature for 30 minutes in an oil bath. Samples were then quenched in liquid nitrogen for 5 minutes before allowing to return to room temperature. The electrolytes were sectioned at -120 °C using RMC Boeckeler PT XL Cryo-Ultramicrotome to obtained an ultrathin film (100 nm). The ultrathin film was transferred to a copper grid with formvar/carbon supporting film and stored in an argon glovebox immediately after cryo microtoming to minimize the effect of humidity. Poly(ethylene oxide)-rich domains were stained to increase contrast and stability under the electron beam by exposing the ultrathin film to ruthenium tetroxide vapor for 25 minutes at room temperature. TEM was performed using a Philips CM 200 transmission electron microscope operating at 200 kV.

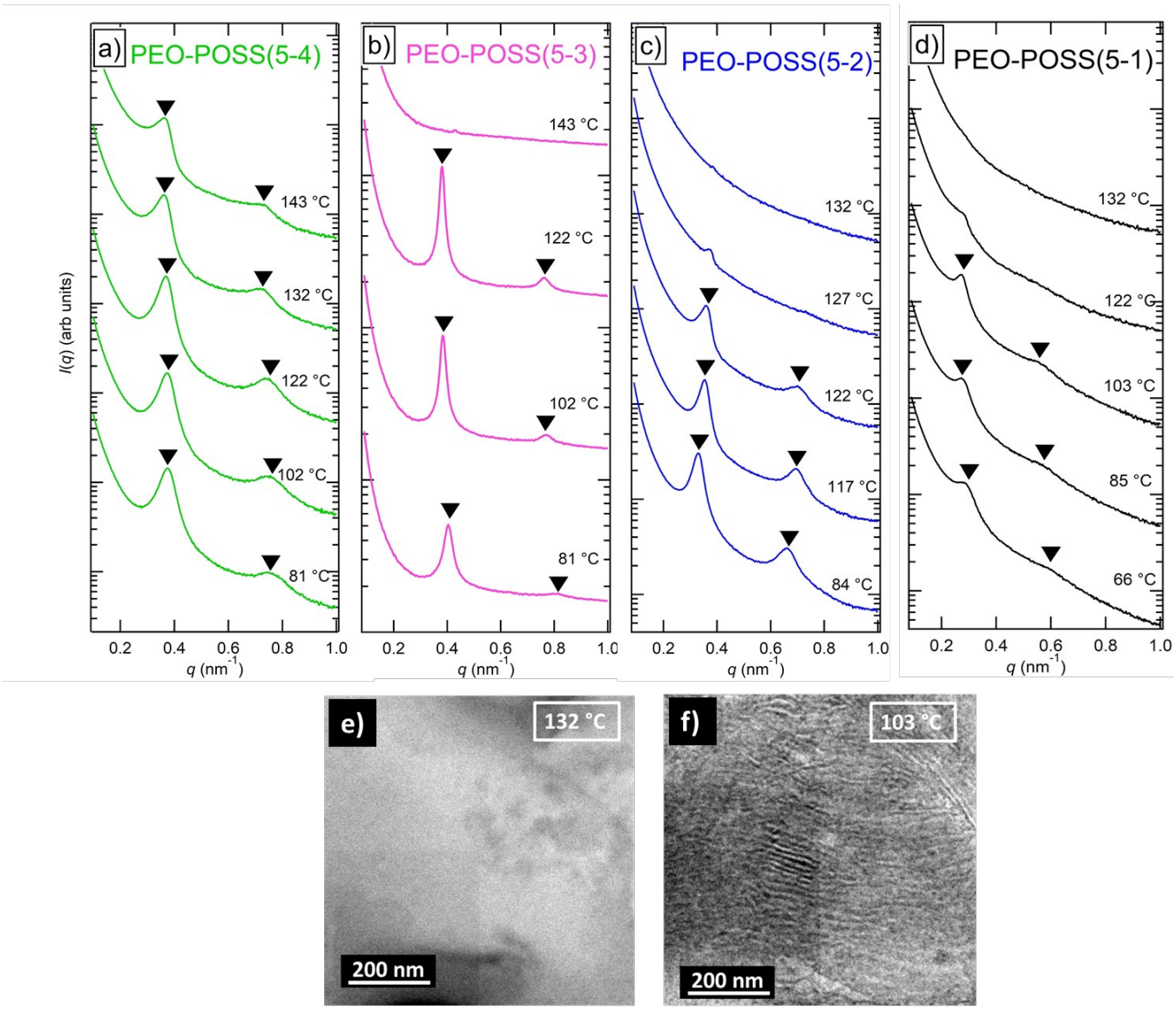

Figure 2. SAXS intensity is plotted as a function of the magnitude of the scattering vector, *q,* for neat PEO-POSS copolymers a) PEO-POSS(5-4) b) PEO-POSS(5-3) c) PEO-POSS(5-2) d) PEO-POSS(5-1). Profiles are shifted vertically. Scans are performed upon cooling from 132 °C to 66 ° C in ~20 °C increments with temperatures indicated on the left. Triangles indicate peaks characteristic of lamellar order (*q**, *2q**). e-f) TEM micrographs of RuO_4 stained PEO-POSS(5-1). Separate samples were heated at 132 ° C e) and 103 ° C f) then quenched using liquid nitrogen. SAXS and TEM are consistent with each other.

RESULTS AND DISCUSSION

Small angle X-ray scattering (SAXS) profiles of neat PEO−POSS at selected temperatures between 66 °C and 143 °C (both blocks are amorphous in this temperature range) are shown in Figure 2a-c where scattering intensity, $I(q)$, is plotted as a function of the magnitude of the scattering vector, q. In Figure 2a, we show data obtained from neat PEO-POSS(5-4). This samples exhibits an ordered lamellar morphology throughout the accessible temperature range. This is indicated by the presence of a primary scattering peak at $q = q^* = 0.37$ nm^{-1} and a higher order peak at $q = 2q^*$ which are standard signatures of a lamellar morphology. The center-to-center distance between adjacent PEO lamellae, or domain spacing, d, of the copolymers can be determined by the equation $d = 2\pi / q^* = 17$ nm. In Figure 2b, at 81 °C, PEO-POSS(5-3) also exhibits two peaks at $q = q^* = 0.4$ nm^{-1} and at $q = 2q^*$ indicating the presence of a lamellar phase. At 102 °C, the intensity of the primary scattering peak increases and sharpens and the second order peak becomes more prominent, indicating better long-range order. At 122 °C, the primary scattering peak and the second order peak increases and sharpens even further, showing that the long-range order improves at higher temperature. The lamellar morphology persists until 143 °C at which these two peaks disappear and instead, a monotonically decaying scattering profiles is seen. Thus, an order-*to*-disorder transition (ODT) occurs in the neat PEO-POSS(5-3) sample at 133 ± 10 °C.

Similarly, in Figure 2c the scattering profiles of PEO-POSS(5-2) indicate a lamellar morphology at 84 °C and 117 °C with peaks at $q^* = 0.37$ and $2q^*$

and domain spacing 17 nm. At 122 °C, the primary scattering peak diminishes in intensity and the second order peak broadens. At 127 °C, the q^* peak decreases in intensity and the $2q^*$ peak disappears completely, indicating an ODT is approaching. This SAXS profiles indicates the presence of disordered concentration fluctuations.[48] At 132 °C, a monotonically decaying scattering profile is seen. It is evident that PEO−POSS(5-2) exhibits an ODT upon heating at 125 ± 3 °C.

In Figure 2d, PEO-POSS(5-1) shows a qualitatively similar profile to PEO-POSS(5-2) (Figure 2c). At 66 °C and 85 °C, we obtain a lamellar morphology with primary scattering peak at $q = q^* = 0.35$ nm^{-1} and a second order scattering peak at $2q^*$ and $d = 18$ nm. The second order scattering peak is broader and poorly defined in comparison to PEO-POSS(5-2) (Figure 2c) and PEO-POSS(5-3) (Figure 2b) indicating weaker segregation between the PEO-rich and POSS-rich phases. At 103 °C both the primary and secondary scattering peaks increase in intensity (similar to PEO-POSS(5-3) at 102 °C and 122 °C (Figure 2b)). At 122 °C, the intensity of the primary scattering peak diminishes significantly and the second order peak disappears as in Figure 2c at 127 °C indicating an ODT at 113 ± 10 °C. The monotonically decaying scattering profile at 132 °C indicates disorder.

Electron microscopy was used to confirm the lamellar and disordered morphologies seen in SAXS in Figure 2e-f. Two PEO-POSS(5-1) samples were annealed at 132 °C (Figure 2e) and 103 °C (Figure 2f), then quenched in liquid nitrogen to “freeze” the morphology at these temperatures. The

resulting micrographs, obtained by transmission electron microscopy (TEM) bright phase represents the RuO_4 stained PEO-rich microphases. The micrograph obtained from the sample quenched at 103 °C shows alternating dark and bright stripes representing the lamellar phase. The micrograph obtained from the sample quenched at 132 °C shows a uniform image phase mixing of PEO-rich and POSS-rich phases, confirming the disordered SAXS scattering profile in Figure 2d at the same temperature. We chose PEO-POSS(5-1) because it is the most asymmetric block copolymer with f_{EO} = 0.84 (see Table 1). In conventional block copolymers, such highly asymmetric systems would exhibit cylindrical or spherical morphologies. The TEM image in Figure 2e confirms our conclusion of a lamellar morphology in PEO-POSS(5-1) based on SAXS (Figure 2d).

The ODTs exhibited by PEO-POSS without salt is qualitatively similar to that of most all-organic diblock copolymers.[49] This suggests that the PEO and POSS chains exhibit repulsive interactions.[50-52] At low temperatures, these interactions dominate, leading to an ordered phase. At high temperatures entropic effects dominate, leading to mixing of PEO and POSS segments.

The sharpness of the lamellar peaks decreases with increasing f_{EO}. This can be seen by comparing the low temperature data in Figures 2a-e. In fact, the higher order peak in PEO-POSS(5-1) is barely visible. It is evident that long-range order decreases as f_{EO} increases from 0.61 to 0.84. This is expected because the lamellae are most often found in symmetric systems.

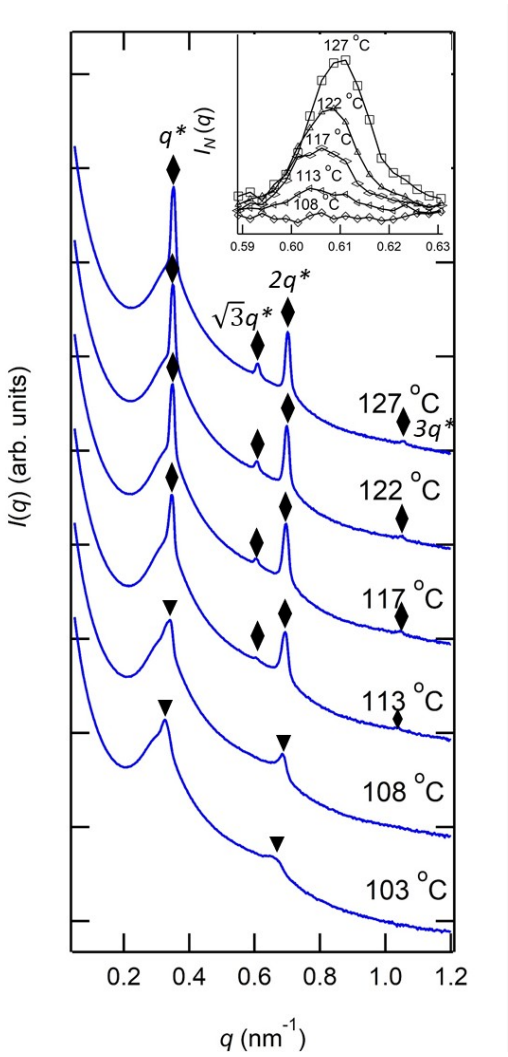

Figure 3. SAXS scattering profiles of PEO-POSS(5-2) r = 0.08 . Scattering intensity is plotted as a function of the magnitude of the scattering vector, q. Profiles are shifted vertically. Scans are performed upon cooling from 127 °C to 103 ° C in ~5 °C increments with temperatures indicated on the right. The inset on the top right is background subtracted $\sqrt{3}q^*$ peak.

The SAXS profiles obtained from a PEO−POSS(5-2)/LiTFSI mixture with r = 0.08 are shown in Figure 3. At 103 °C and 108 °C, the scattering profile exhibits two peaks at $q = q^* = 0.35$ nm^{-1} and at $q = 2q^*$ denoted with triangles indicating lamellar morphology. Increasing the temperature to 113 °C results in the emergence of an additional scattering peak at $q = \sqrt{3}q^*$

denoted with a diamond that is superimposed on the scattering profile of the lamellar phase. A peak at $q = \sqrt{3}q^*$ is a standard signature of a hexagonally packed cylinders morphology. It is difficult to see this peak in the intensity versus q data shown in Figure 3. In order to clarify the presence of the $\sqrt{3}q^*$ peak, we define a normalized scattering intensity in equation 5 as outlined in ref [53]

$$I_N(q) = \frac{I(q)}{I(q)\,at\,T = 84°C}. \quad [5]$$

The normalized scattering profile in the vicinity of the $\sqrt{3}q^*$ peak is shown in the inset at the top right of Figure 3 at temperatures between 108 °C and 127 °C. The normalized scattering peak at 108 °C is featureless. However, a clear signature of the $\sqrt{3}q^*$ peak is seen to grow in at higher temperatures (≥ 113 °C). In ref [45], we used electron tomography to show that SAXS profiles with the sqrt 3 peak indicate the presence of coexisting lamellae and hexagonally packed cylinders. In PEO-POSS(5-2) r = 0.08 the transition from lamellae to this coexisting phase at 108 ± 3 °C.

The primary SAXS peaks in Figure 3 comprise a sharp peak superposed on a broad background. The importance of the background decreases with increasing temperatures. The background is most prominent at 103 °C and least prominent at 127 °C. The background may arise from form factor

contributions to the scattering profiles or from fluctuations in salt concentrations within the ordered domains. The electron tomography results given in ref [45] rule out the possibility of coexisting disordered and ordered phases. This background is seen in all of the PEO-POSS/LiTFSI mixtures.

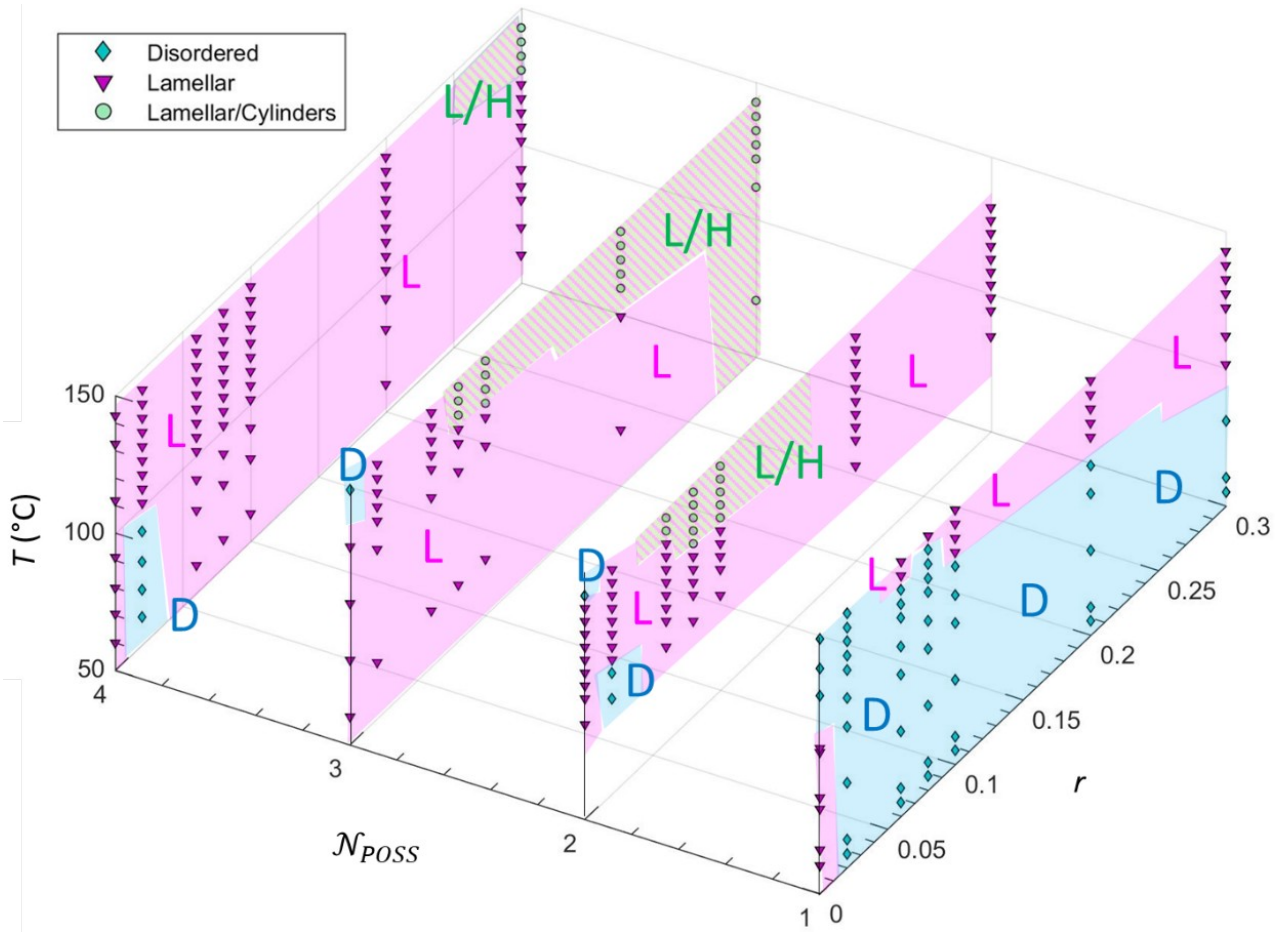

Figure 4. Phase diagram of PEO-POSS electrolytes summarizing morphology data determined by SAXS shown as a function salt concentration, *r*, number of POSS units N_{POSS}, and temperature, *T*. The blue diamonds, purple triangles, and green circles represent morphological data from SAXS. The shaded regions represent the disordered (D), lamellae(L), and coexisting lamellae and hexagonally packed cylinder (L/H) phases respectively.

The SAXS profiles shown in Figures 2 and 3 are representative of data obtained from all of our PEO-POSS without salt and PEO-POSS/LiTFSI mixtures. Depending on salt concentration, temperature, and block copolymer composition, we obtain 3 phases: disorder (D), lamellar (L), and coexisting lamellar/hexagonally packed cylinders (L/H). Figure 4 summarizes the results of the SAXS experiments, where the morphologies of PEO−POSS/LiTFSI mixtures are shown as a function of salt concentration, number of POSS units (N_{POSS}), and temperature. The data from each copolymer is separately shown on individual panels in Figure 4. We discuss each panel separately:

1) At N_{POSS} = 1, a lamellar to disorder transition upon heating is seen in the neat block copolymer. The addition of salt leads to the emergence of a wide disordered window and lamellar phases are seen at high salt concentrations and high temperatures.

2) At N_{POSS} = 2, a disorder to lamellar transition upon heating is seen in the neat copolymer. A small disordered pocket is seen at r = 0.02 that gives way to a lamellar phase upon heating. The lamellar phase is seen over a wide window with L/H coexistence at intermediate salt concentrations and high temperatures.

3)The data at N_{POSS} = 3 is similar to N_{POSS} = 2 except for the absence of a disordered pocket at r = 0.02. A wide lamellar window is seen with L/H

coexistence at high temperatures. At r = 0.30, L/H is seen at all temperatures.

4) At N_{POSS} = 4, the neat polymer is ordered over the entire temperature window, a small disordered pocket is seen at r = 0.02 (similar to N_{POSS} = 2 but different from N_{POSS} = 3). The lamellar phase occupies most of the temperatures and salt concentration window. L/H is only seen at the highest salt concentrations at temperatures above 122 °C.

The phase behavior seen in Figure 4 is extremely complex and very different from conventional block copolymer electrolytes.[54] Developing a coherent framework for presenting all of these data on a single, unified plot is challenging. In this paper, we restrict our attention to the electrolytes in Figure 4 ($r \geq 0.02$). A framework that includes the neat block copolymers is outside the scope of this paper. Our framework is built upon an expression for the effective Flory Huggins interaction parameter, χ_{eff}, that depends on temperature and salt concentration.

A standard approach for determining χ in neat block copolymer melts is through the use of the Leibler's Random Phase Approximation (RPA) which describes scattering from concentration fluctuations in disordered systems.[48,54,55] We adopt this approach to determine χ_{eff} for salt-containing PEO-POSS. The scattering function $I_{dis}(q)$ proposed by Leibler[48] for a monodisperse AB diblock copolymer can be written as follows

$$I_{dis}(q)=C\left[\frac{S(q)}{W(q)}-2\chi_{eff}\right]^{-1}.[6]$$

The only difference between equation 6 and that given by Leibler is the introduction of χ_{eff} instead of χ. $W(q)$ and $S(q)$ are the determinant and sum of the elements, respectively, of the structure factor matrix $\|Sij\|$. The expressions $W(q)$ and $S(q)$ are given by

$$W(q)=S_{AA}(q)S_{BB}(q)-S_{AB}{}^{2}(q)[7]$$

$$S(q)=S_{AA}(q)+S_{BB}(q)+2S_{AB}(q)[8]$$

Where S_{AA}, S_{AB}, and S_{BB} are the pairwise elements of the structure factor matrix

$$S_{AA}(q)=NP_{EO(q)}[9]$$

$$S_{BB}(q)=NP_{POSS(q)}[10]$$

$$S_{AB}(q)=\frac{N}{2}\left[P_{Total}-P_{EO}-P_{POSS}\right].[11]$$

$P_{EO}(q)$ is the form factor of the PEO block which we model as Gaussian chain

49

$$P_{EO}=\frac{2}{x^2}\left[f_{EO/LiTFSI}\,x+e^{-f_{EO/LiTFSI}\,x}-1\right][12]$$

$$x=q^2R_g^2[13]$$

$$R_g^2=\frac{Na^2}{6}[14]$$

where R_g is the radius of gyration of the copolymer. We consider the PEO block and LiTFSI to be one component and POSS to be the other component. $P_{POSS}(q)$ is the form factor of the POSS block which we model as rodlike chain[56]

$$P_{POSS}(q)=\frac{2}{x^2}\left[f_{POSS}\,x+e^{-f_{POSS}\,x}-1\right]+\frac{1}{15\,x\,f_{POSS}N}¿$$

$P_{total}(q)$ is the form factor of the entire chain which we model as Gaussian chain.

$$P_{total}(q)=\frac{2}{x^2}\left[x+e^{-x}-1\right].[16]$$

This is clearly an approximation. In the Supporting Information we show results obtained with $P_{total}(q)$ given by the rodlike chain (equation 15 with f_{POSS} = 1). The final results we obtain are virtually indistinguishable. We thus use equation 16 in our analysis below.

C in equation 6 is the electron density contrast between the PEO/LiTFSI and POSS given by

$$C = v_{ref}\left[B^{\square}_{EO/LiTFSI} - B_{POSS}\right]^2 [17]$$

where v_{ref} is the same reference volume of 0.1 nm^3 used to define N, N_{POSS}, N_{PEO}, and χ_{eff}; $B^{\square}_{EO/LiTFSI}$and B_{POSS} are the scattering length density of EO/LiTFSI and POSS, respectively. $B^{\square}_{EO/LiTFSI}$scattering length density is calculated as follows

$$B^{\square}_{EO/LiTFSI} = Y_{LiTFSI} B_{LiTFSI} + \left(1 - Y_{LiTFSI}\right) B_{EO} [18]$$

where B_i is given by

$$B_i = \frac{r_e n_i N_{AVG} \rho_i}{M_i} [19]$$

and Y_{LiTFSI} is the volume fraction of LiTFSI in the PEO/LiTFSI microphase calculated by

$$Y_{LiTFSI} = \frac{r M_{LiTFSI} \rho_{EO}}{r M_{EO} \rho_{LiTFSI} + r M_{LiTFSI} \rho_{EO}}. [20]$$

In equation 19, r_e is the cross-sectional scattering radius of a free electron; n_i is the number of electrons per i; N_{AVG} is Avogadro's number; ρ_i is the density of i; and M_i is the molar mass of i. The density of the EO/LiTFSI calculation is shown in ref [46].

In principle, equations 6-20 can be used to predict the scattering from a PEO-POSS/LiTFSI mixture with χ_{eff} and R_g as fitting parameters. When this was done, we found systematic disagreement between theory and experiment. We found that the agreement between theory and experiment improved considerably if the contrast term were also used as an additional fitting parameter. Our analysis thus is based on three parameter fits. The average deviation between C and C_{fit} is 8% as shown in the Supporting Information (Figure S5). This suggests that our simplification of combining EO and LiTFSI may not be strictly accurate.

It is evident from Figures 2 and 3 that the scattering peaks are superposed on a monotonically decaying background. We use the following expression to estimate this background

$$I_{bkg}(q) = x\,q^{y} + z \quad [21]$$

where x, y and z are simply fitting parameters. The experimental scattering profiles that we analyze below are obtained after background subtraction.

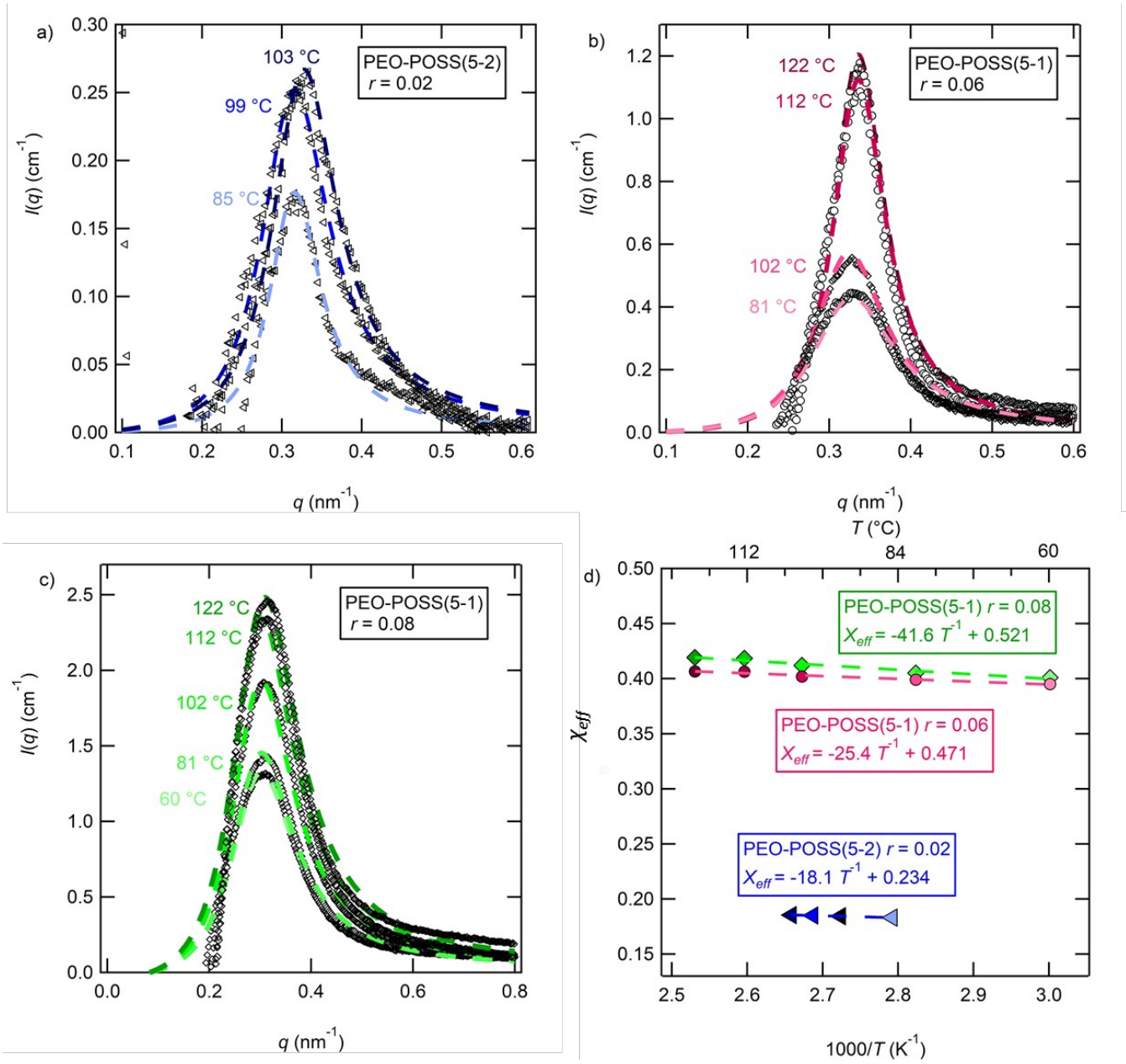

Figure 5. a) SAXS intensity profile for PEO-POSS(5-2) with salt concentration at r = 0.02 at various temperatures and the corresponding RPA fits (dashed line). b) PEO-POSS(5-1) r = 0.06 c) PEO-POSS(5-1) r = 0.08 d) χ_{eff} plotted as a function of inverse temperature.

Typical background subtracted scattering profiles of disordered PEO-POSS/LiTFSI mixtures are shown in Figures 5a-c. The RPA fits are shown by dashed lines in these figures. Figure 5a shows disordered SAXS scattering profiles of PEO-POSS(5-2) r = 0.02 between 85 and 103 °C in the vicinity of q^*. The dashed lines are the RPA fits to the scattering data. Here, the fits conform well to the data. The q^* peak at 85 °C exhibits maximum absolute scattering intensity of 0.18 cm^{-1} corresponding to a fitted χ_{eff} = 0.1830. The peak grows with increasing temperature; the q^* peak at 103 °C exhibits maximum absolute scattering intensity of 0.22 cm^{-1} which corresponds to a slightly increased value of χ_{eff} = 0.1854. Similar trends are seen in Figure 5b for the case of PEO-POSS(5-1) r =0.06 and Figure 5c for the case of PEO-POSS(5-1) r = 0.08. In Figure 5b, the primary scattering peak grows in intensity between 81 °C to 122 °C. In Figure 5c, the primary scattering peak grows in intensity between 60 °C to 122 °C.

The dependence of χ_{eff} on temperature for the three disordered electrolytes discussed in the preceding paragraph is shown in Figure 5d. We use the standard form for determining the temperature dependence of χ_{eff}.

$$\chi_{eff} = A + \frac{B}{T} \quad [22]$$

The dashed lines in Figure 5d are fits of equation 22 which give parameters A and B. Note that B is negative for all cases. The temperature dependence of χ_{eff} is weak relative to the dependence of salt concentration. χ_{eff} increases by a factor of 2.4 when r is increased from 0.02 to 0.06 (see Figure 5d). In contrast, χ_{eff} only

increases by a factor of about 1.004 over the accessible temperature range. Interestingly, increasing r from 0.06 to 0.08 results in a modest increase in χ_{eff}.

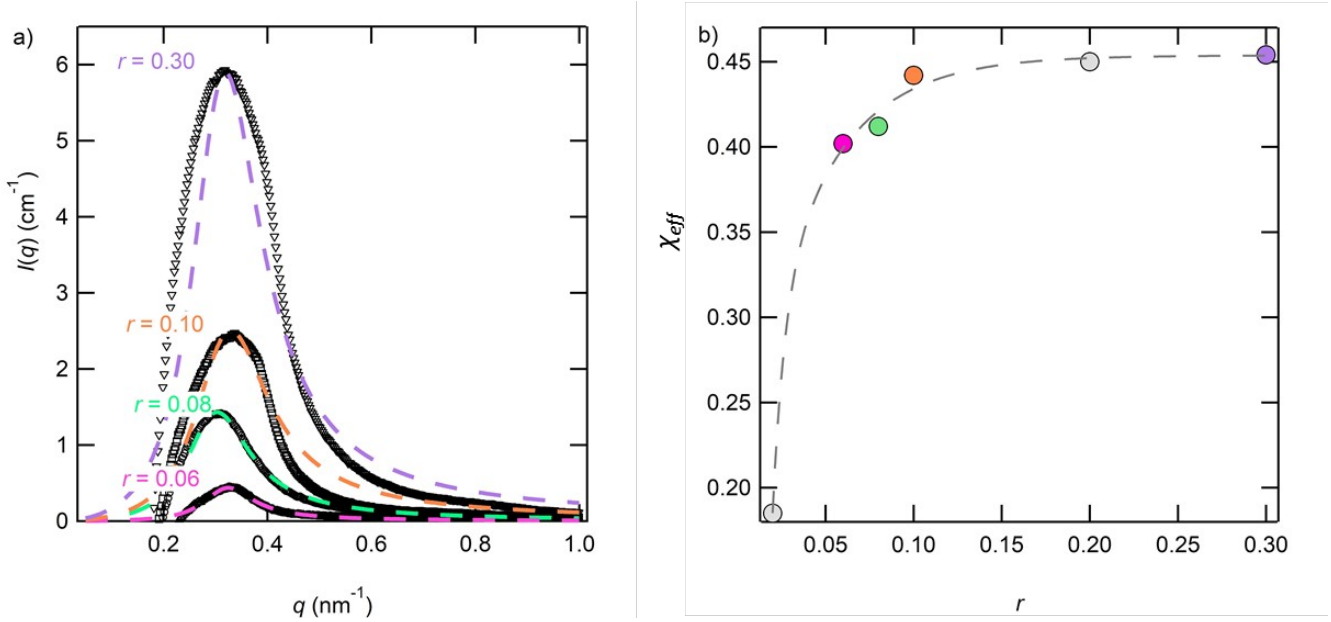

Figure 6. a) SAXS intensity is plotted as a function of the magnitude of the scattering vector, q, in PEO-POSS(5-1) with salt concentration at r = 0.06 to r = 0.30 and the corresponding RPA fits (dashed line) at 60 °C. b) χ_{eff} versus salt concentration at 60 °C. The colored markers correspond to values obtained by RPA fits in a). The dashed line is the fit to equation 23.

The analysis described in the preceding paragraph was applied to all disordered PEO-POSS/LiTFSI mixtures with $r \geq 0.02$. In most cases, the agreement between theory and experiment was similar to that show in Figure 5. The largest disagreements were seen in PEO-POSS(5-1). in Figure 6a we show disordered state scattering profiles from this electrolyte at selected values of r and at a fixed temperature at 60 °C. The values of χ_{eff} obtained from this analysis is shown in Figure 6b. It is evident that χ_{eff} increases rapidly with increasing r at low values of r ($r < 0.08$). The increase in χ_{eff} from r = 0.1 to r = 0.3 is less dramatic.

The data in Figure 6b is fit to an exponential equation plotted as a dashed line through the points.

$$\chi_{eff} = C + D e^{-Er} + F e^{-Gr} \quad [23]$$

Where C, D, E, F, and G are empirically determined fitting parameters.

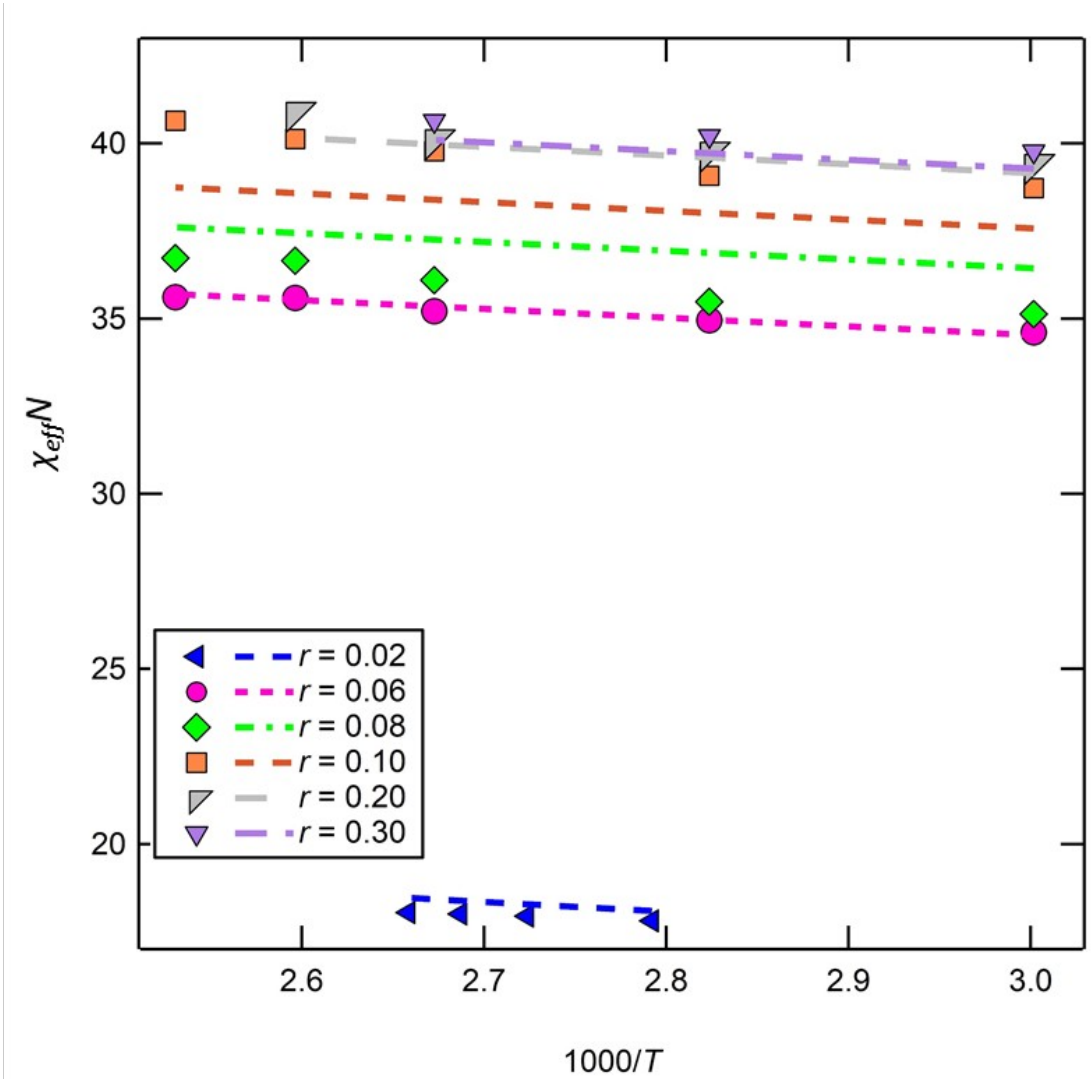

Figure 7. Effective segregation strength $\chi_{eff}N$ plotted as a function of inverse temperature for a range of salt concentrations r = 0.02, r = 0.06, r = 0.08. Dashed lines indicate predictions based on equation 24. For the given value of r the colors of the dashed lines correspond to the markers of the same color.

Combining equations 22 and 23 we obtain the following expression for the dependence of χ_{eff} on T and r

$$\chi_{eff}(T,r)=A+\frac{B}{T\left(K^{-1}\right)}+C-De^{-Er}-Fe^{-Gr}.[24]$$

The empirically determined constants *A*-*G* are given in Table 2.

Table 2. The best-fit double exponential equation parameters of all χ_{eff} in PEO-POSS electrolytes

A	B	C	D	E	F	G
8.0103×10^{-2}	2.8001×10^{-2}	4.55436×10^{-1}	2.4756×10^{-1}	2.5361×10^{-1}	2.3153	1.4824×10^{2}

In Figure 7 we compare experimentally determined dependence of segregation strength ($\chi_{eff}N$) on temperature and salt concentration with the prediction based on equation 24. The dashed lines in Figure 7 indicate the $\chi_{eff}N$ calculated from equation 24 in the same color as the data points which they represent. It is evident that equation 24 provides a reasonable description of all measured values of $\chi_{eff}N$.

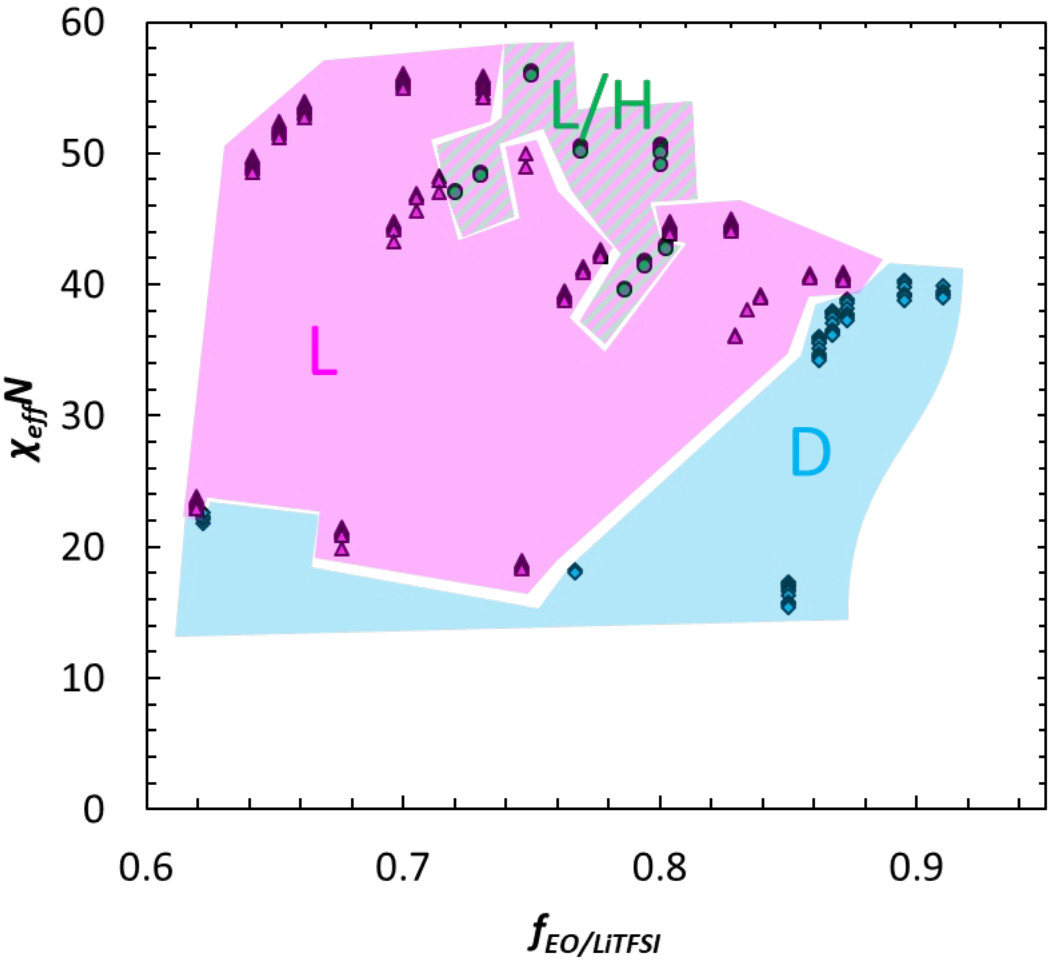

Figure 8. Morphology data for PEO-POSS block copolymer electrolytes plotted as a function of $\chi_{eff}N$ versus volume fraction of the salt containing phase, $f_{EO/LiTFSI}$. Lamellar (L) and disordered (D) regions are shaded pink and blue respectively. Coexistence of lamellae and hexagonally packed cylinders (L/H) is denoted by hatched colored regions.

The morphology data determined via SAXS for all PEO-POSS/LiTFSI mixtures, presented in Figure 4 on a three-dimensional plot, are recast in Figure 8 on a two-dimensional plot of $\chi_{eff}N$ calculated from expression 24 as the y-axis and $f_{EO/LiTFSI}$ as the x-axis. Figures 4 and 8 use the same color scheme. The phase diagram (Figure 8) is dominated by the lamellar phase which is found in the range $0.60 \leq f_{EO/LiTFSI} \leq 0.85$ and $20 \leq \chi_{eff}N \leq 50$. A

pocket of coexisting hexagonally packed cylinders/lamellae is found in the range $0.72 \leq f_{EO/LiTFSI} \leq 0.81$ and $37 \leq \chi_{eff}N \leq 58$. The lower portion of the phase diagram ($0 \leq \chi_{eff}N \leq 20$) is largely disordered. This disordered phase exists up to $\chi_{eff}N$ up to 40. It is perhaps interesting to note that all of the complexity seen in the three-dimensional phase diagram in Figure 4 maps onto contiguous regions on the $\chi_{eff}N$ versus $f_{EO/LiTFSI}$ plot. This was made possible by our analysis of scattering in the disordered state which led to equation 24.

CONCLUSION

We have studied the effect of salt addition on the self-assembly behavior of inorganic-organic PEO-POSS block copolymer electrolytes. We report on the phase behavior of PEO-POSS/LiTFSI mixtures with volume fraction, $f_{EO/LiTFSI}$ ranging from 0.61 to 0.91, chain length, N, ranging from 88 to 121, temperatures from 60 to 143 °C, and salt concentration from $r = 0.02$ to 0.30. Without salt, PEO−POSS presents a classical order-to-disorder transition upon heating. The addition of salt at low concentration ($r \leq 0.02$) results in the stabilization of the disordered phase. However, further increase in salt concentration results in the stabilization of ordered phases. The segregation strength of the polymer electrolytes ($\chi_{eff}N$) is determined by analyzing disordered scattering profiles using Leibler's Random Phase Approximation.[48] The PEO block was modeled as a flexible Gaussian chain

while the POSS block was modeled as a rodlike chain. The results obtained from electrolytes with $r \geq 0.02$ are summarized on a phase diagram that shows the dependence of the ordered morphology on $\chi_{eff}N$ and $f_{EO/LiTFSI}$. The only two types of ordered phase were found: lamellae and coexisting lamellae/hexagonally packed cylinders. Further work on understanding the molecular origins of the observed phase behavior of PEO-POSS/LiTFSI seems warranted.

ACKNOWLEDGEMENTS

This work was supported by the Assistant Secretary for Energy Efficiency and Renewable Energy, Office of Vehicle Technologies of the U.S. Department of Energy under Contract DE-AC02-05CH11231 under the Battery Materials Research Program. Funding for the electron tomography work was provided by the Soft Matter Electron Microscopy Program, supported by the Office of Science, Office of Basic Energy Science, U.S. Department of Energy, under Contract No. DE- AC02-05CH11231. The electron microscopy work was performed at Donner Lab, and the X-ray work was performed at Advanced Light Source, which is a DOE Office of Science User Facility, was supported by Contract No. DE-AC02- 05CH11231. Work at the Stanford Synchrotron Radiation Light Source, a user facility at SLAC National Accelerator Laboratory, was supported by the U.S. Department of Energy, Office of Science, Office of Basic Energy Sciences under Contract No. DE-AC02-

76SF00515. Work at the Molecular Foundry was supported by the Office of Science, Office of Basic Energy Sciences, of the U.S. Department of Energy under Contract No. DE-AC02-05CH11231. G.K.S. acknowledges funding from a National Science Foundation Graduate Student Research Fellowship.

LIST OF SYMBOLS

a statistical segment length (nm)

B_i scattering length density of species i

d domain spacing (nm)

$Đ$ dispersity

f_i volume fraction of the species i

$f_{EO/LiTFSI}$ volume fraction of PEO/LiTFSI microphase

I scattering intensity

I_{dis} disordered scattering intensity (cm^{-1})

I_{bkg} background scattering intensity (cm^{-1})

M_{PEO} molecular weight of the poly(ethylene oxide) block (kg mol^{-1})

M_{PPOSS} molecular weight of the polyhedral oligomeric silsesquioxane block (kg mol^{-1})

M_i molecular weight of species i (g mol^{-1})

N degree of polymerization

N_i degree of polymerization of species i

N_{POSS} number of POSS units

q scattering vector (nm^{-1})

q^* scattering vector at the primary scattering peak (nm^{-1})

r salt concentration ($[Li^+]\,[EO]^{-1}$)

R_g radius of gyration (nm)

T Temperature (°C)

Y volume fraction salt in PEO/LiTFSI microphase (LiTFSI cm^3 PEO/LiTFSI cm^{-3})

GREEK

ν_i molar volume of species *i* (cm^3 mol^{-1})

ν_{ref} reference volume of species *i* (cm^3 mol^{-1})

ρ_i density of species *i* (g cm^{-1})

 x-ray scattering angle

λ x-ray wavelength

χ Flory-Huggins interaction parameter

χ_{eff} Flory-Huggins interaction parameter of PEO-POSS/LiTFSI

ASSOCIATED CONTENT

Supporting Information. NMR, GPC, TGA, DSC, experimental fitting, calculated contrast values.

AUTHOR INFORMATION

Corresponding Authors

*Irune Villaluenga

irvillaluenga@gmail.com

*Nitash P. Balsara

nbalsara@berkeley.edu

Author Contributions

The manuscript was written through contributions of all authors. All authors have given approval to the final version of the manuscript.

REFERENCES

1. Armand, M. & Tarascon, J. M. Building better batteries. Nature 451, 652–657 (2008).

2. Xie, S. & Lodge, T. P. Phase Behavior of Binary Polymer Blends Doped with Salt. Macromolecules 51, 266–274 (2018).

3. Huang, J., Tong, Z. Z., Zhou, B., Xu, J. T. & Fan, Z. Q. Phase behavior of LiClO4-doped poly(ε-caprolactone)-b- poly(ethylene oxide) hybrids in the presence of competitive interactions. Polymer (Guildf). 55, 1070–1077 (2014).

4. Young, W. S. & Epps, T. H. Salt doping in PEO-containing block copolymers: Counterion and concentration effects. Macromolecules 42, 2672–2678 (2009).

5. Zardalidis, G., Gatsouli, K., Pispas, S., Mezger, M. & Floudas, G. Ionic Conductivity, Self-Assembly, and Viscoelasticity in Poly(styrene-b-ethylene oxide) Electrolytes Doped with LiTf. Macromolecules 48, 7164–7171 (2015).

6. Wang, J. Y., Chen, W. & Russell, T. P. Ion-complexation-induced changes in the interaction parameter and the chain conformation of PS-b-PMMA copolymers. Macromolecules 41, 4904–4907 (2008).

7. Naidu, S., Ahn, H., Gong, J., Kim, B. & Ryu, D. Y. Phase behavior and ionic conductivity of lithium perchlorate-doped polystyrene-b-poly(2-vinylpyridine) copolymer. Macromolecules 44, 6085–6093 (2011).

8. Irwin, M. T., Hickey, R. J., Xie, S., Bates, F. S. & Lodge, T. P. Lithium Salt-Induced Microstructure and Ordering in Diblock Copolymer/Homopolymer Blends. Macromolecules 49, 4839–4849 (2016).

9. Wang, X., Goswami, M., Kumar, R., Sumpter, B. G. & Mays, J. Morphologies of block copolymers composed of charged and neutral blocks. Soft Matter 8, 3036–3052 (2012).

10. Gomez, E. D., Panday, A., Feng, E. H., Chen, V., Stone, G. M., Minor, A. M., Kisielowski, C., Downing, K. H., Borodin, O., Smith, G. D. & Balsara, N. P. Effect of ion distribution on conductivity of block copolymer electrolytes. Nano Lett. 9, 1212–1216 (2009).

11. Besner, S., Vallée, A. & Bouchard, G. Effect of Anion Polarization on Conductivity Behavior of Poly(ethylene oxide) Complexed with Alkali Salts. Macromolecules 25, 6480–6488 (1992).

12. Hu, H., Gopinadhan, M. & Osuji, C. O. Directed self-Assembly of block copolymers: A tutorial review of strategies for enabling nanotechnology with soft matter. Soft Matter 10, 3867–3889 (2014).

13. Hou, K. J. & Qin, J. Solvation and Entropic Regimes in Ion-Containing Block Copolymers. Macromolecules 51, 7463–7475 (2018).

14. Grzetic, D. J., Delaney, K. T. & Fredrickson, G. H. The effective χ parameter in polarizable polymeric systems: One-loop perturbation theory and field-theoretic simulations. J. Chem. Phys. 148, (2018).

15. Sethuraman, V., Mogurampelly, S. & Ganesan, V. Multiscale Simulations of Lamellar PS-PEO Block Copolymers Doped with LiPF6Ions. Macromolecules 50, 4542–4554 (2017).

16. Kim, S. K., Kim, D. G., Lee, A., Sohn, H. S., Wie, J. J., Nguyen, N. A., MacKay, M. E. & Lee, J. C. Organic/inorganic hybrid block copolymer electrolytes with nanoscale ion-conducting channels for lithium ion batteries. Macromolecules 45, 9347–9356 (2012).

17. Liu, Y., Ma, X., Sun, K., Yang, K. & Chen, F. Preparation and characterization of gel polymer electrolyte based on electrospun polyhedral oligomeric silsesquioxane-poly(methyl methacrylate)8/polyvinylidene fluoride hybrid nanofiber membranes for lithium-ion batteries. J. Solid State Electrochem. 22, 581–590 (2018).

18. Zhang, J., Ma, C., Liu, J., Chen, L., Pan, A. & Wei, W. Solid polymer electrolyte membranes based on organic/inorganic nanocomposites with star-shaped structure for high performance lithium ion battery. J. Memb. Sci. 509, 138–148 (2016).

19. Lee, J. Y., Lee, Y. M., Bhattacharya, B., Nho, Y. C. & Park, J. K. Solid polymer electrolytes based on crosslinkable polyoctahedral silsesquioxanes (POSS) for room temperature lithium polymer batteries. J. Solid State Electrochem. 14, 1445–1449 (2010).

20. Polu, A. R. & Rhee, H. W. Nanocomposite solid polymer electrolytes based on poly(ethylene oxide)/POSS-PEG (n=13.3) hybrid nanoparticles for lithium ion batteries. J. Ind. Eng. Chem. 31, 323–329 (2015).

21. Jothibasu, S., Chandramohan, A., Kumar, A. A. & Alagar, M. Polyhedral oligomeric silsesquioxane (POSS) reinforced-unsaturated polyester hybrid nanocomposites: Thermal, thermomechanical and morphological properties. J. Macromol. Sci. Part A Pure Appl. Chem. 55, 433–439 (2018).

22. Romo-Uribe, A. Viscoelastic Behavior of Unentangled POSS–Styrene Nanocomposites and the Modification of Macromolecular Dynamics. Macromolecules acs.macromol.7b01645 (2017).

23. Yu, C. Bin, Ren, L. J. & Wang, W. Synthesis and Self-Assembly of a Series of nPOSS-b-PEO Block Copolymers with Varying Shape Anisotropy. Macromolecules 50, 3273–3284 (2017).

24. Lichtenhan, J. D., Otonari, Y. A. & Carr, M. J. Linear Hybrid Polymer Building Blocks: Methacrylate-Functionalized Polyhedral Oligomeric Silsesquioxane Monomers and Polymers. Macromolecules 28, 8435–8437 (1995).

25. Tada, Y., Yoshida, H., Ishida, Y., Hirai, T., Bosworth, J. K., Dobisz, E., Ruiz, R., Takenaka, M., Hayakawa, T. & Hasegawa, H. Directed self-assembly of POSS containing block copolymer on lithographically defined chemical template with morphology control by solvent vapor. Macromolecules 45, 292–304 (2012).

26. Miao, J., Cui, L., Lau, H. P., Mather, P. T. & Zhu, L. Self-assembly and chain-folding in hybrid coil-coil-cube triblock oligomers of polyethylene-b-

poly(ethylene oxide)-b-polyhedral oligomeric silsesquioxane. Macromolecules 40, 5460–5470 (2007).

27. Zheng, L., Waddon, A. J., Farris, R. J. & Coughlin, E. B. X-ray characterizations of polyethylene polyhedral oligomeric silsesquioxane copolymers. Macromolecules 35, 2375–2379 (2002).

28. Huang, M., Yue, K., Huang, J., Liu, C., Zhou, Z., Wang, J., Wu, K., Shan, W., Shi, A. C. & Cheng, S. Z. D. Highly Asymmetric Phase Behaviors of Polyhedral Oligomeric Silsesquioxane-Based Multiheaded Giant Surfactants. ACS Nano 12, 1868–1877 (2018).

29. Chae, C. G., Yu, Y. G., Seo, H. Bin, Kim, M. J., Grubbs, R. H. & Lee, J. S. Experimental Formulation of Photonic Crystal Properties for Hierarchically Self-Assembled POSS-Bottlebrush Block Copolymers. Macromolecules 51, 3458–3466 (2018).

30. Kato, F., Sugimoto, S., Chandra, A. & Hayakawa, T. Morphology control and inducing a curvature on the domain interface by increasing the steric bulk of polymethacrylate in POSS-containing diblock copolymers. J. Polym. Sci. Part A Polym. Chem. 55, 2234–2242 (2017).

31. Zhu, B. L., Cheng, S. Z. D., Huang, P., Ge, Q., Quirk, R. P., Thomas, E. L., Lotz, B., Hsiao, B. S., Yeh, F. & Liu, L. Nanoconfined Polymer Crystallization in the Hexagonally Perforated Layers of a Self- Assembled PS-b-PEO Diblock Copolymer. 31–34 (2002).

32. Hirai, T., Leolukman, M., Liu, C. C., Han, E., Kim, Y. J., Ishida, Y., Hayakawa, T., Kakimoto, M. A., Nealey, P. F. & Gopalan, P. One-step direct-patterning template utilizing self-assembly of POSS-containing block copolymers. Adv. Mater. 21, 4334–4338 (2009).

33. Zheng, Y., Wang, L., Yu, R. & Zheng, S. Synthesis and self-assembly behavior of organic-inorganic poly(ethylene oxide)-block-poly(MA POSS)-block-poly(N-isopropylacrylamide) triblock copolymers. Macromol. Chem. Phys. 213, 458–469 (2012).

34. Haddad, T. S., Mather, P. T., Jeon, H. G., Chun, S. B. & Phillips, S. H. Hybrid Inorganic/Organic Diblock Copolymers. Nanostructure in Polyhedral Oligomeric Silsesquioxane. Mater. Res. 609, 1–6 (2000).

35. Yue, K., Liu, C., Guo, K., Yu, X., Huang, M., Li, Y., Wesdemiotis, C., Cheng, S. Z. D. & Zhang, W. Bin. Sequential ‘click’ approach to polyhedral oligomeric silsesquioxane-based shape amphiphiles. Macromolecules 45, 8126–8134 (2012).

36. Shimada, T., Doi, M. & Okano, K. Concentration fluctuation of stiff polymers. I. Static structure factor. J. Chem. Phys. 88, 2815–2821 (1988).

37. Olsen, B. D. & Segalman, R. A. Nonlamellar phases in asymmetric rod-coil block copolymers at increased segregation strengths. Macromolecules 40, 6922–6929 (2007).

38. Olsen, B. D. & Segalman, R. A. Structure and thermodynamics of weakly segregated rod-coil block copolymers. Macromolecules 38, 10127–10137 (2005).

39. Chen, J. T., Thomas, E. L., Ober, C. K. & Hwang, S. S. Zigzag Morphology of a Poly(styrene-b-hexyl isocyanate) Rod-Coil Block Copolymer. Macromolecules 28, 1688–1697 (1995).

40. Hammouda, B. SANS from homogeneous polymer mixtures: A unified overview. Polym. Charact. 106, 87–133 (1993).

41. Hammouda, B. Analysis of the Beaucage model. J. Appl. Crystallogr. 43, 1474–1478 (2010).

42. Flory, P. J. Statistical Thermodynamics of Semi-Flexible Chain Molecules. Proc. R. Soc. A Math. Phys. Eng. Sci. 234, 60–73 (1956).

43. Benmouna, M., Akcasu, A. Z. & Daoud, M. Effect of Stiffness on the First Cumulant and Polymer Dimensions in Solution. Macromolecules 13, 1703–1712 (1980).

44. Holyst, R. & Schick, M. Copolymers as amphiphiles in ternary mixtures: An analysis employing disorder, equimaxima, and Lifshitz lines. J. Chem. Phys. 96, 7728–7737 (1992).

45. Sethi, G. K., Jiang, X., Chakraborty, R., Loo, W. S., Villaluenga, I. & Balsara, N. P. Anomalous Self-Assembly and Ion Transport in Nanostructured Organic–Inorganic Solid Electrolytes. ACS Macro Lett. 1056–1061 (2018).

46. Pesko, D. M., Timachova, K., Bhattacharya, R., Smith, M. C., Villaluenga, I., Newman, J. & Balsara, N. P. Negative Transference Numbers in Poly(ethylene oxide)-Based Electrolytes. J. Electrochem. Soc. 164, E3569–E3575 (2017).

47. Ilavsky, J. Nika: Software for two-dimensional data reduction. J. Appl. Crystallogr. 45, 324–328 (2012).

48. Leibler, L. Theory of Microphase Separation in Block Copolymers. Macromolecules 13, 1602–1617 (1980).

49. Teran, A. A. & Balsara, N. P. Thermodynamics of block copolymers with and without salt. J. Phys. Chem. B 118, 4–17 (2014).

50. Bates, F. S. & Fredrickson, G. H. Block Copolymer Thermodynamics: Theory and Experiment. Annu. Rev. Phys. Chem. 41, 525–557 (1990).

51. Bates, F. S., Rosedale, J. H. & Fredrickson, G. H. Fluctuation effects in a symmetric diblock copolymer near the order-disorder transition. *The Journal of Chemical Physics* **92,** 6255–6270 (1990).

52. Balsara, N. P., Jonnalagadda, S. V., Lin, C. C., Han, C. C. & Krishnamoorti, R. Thermodynamic interactions and correlations in mixtures of two homopolymers and a block copolymer by small angle neutron scattering. J. Chem. Phys. 99, 10011–10020 (1993).

53. Hahn, H., Eitouni, H. B., Balsara, N. P. & Pople, J. A. Responsive Solids from Cross-Linked Block Copolymers. Phys. Rev. Lett. 90, 4 (2003).

54. Cochran, E. W., Garcia-Cervera, C. J. & Fredrickson, G. H. Stability of the gyroid phase in diblock copolymers at strong segregation. Macromolecules 39, 2449–2451 (2006).

55. Fredrickson, G. H. & Helfand, E. Fluctuation effects in the theory of microphase separation in block copolymers. J. Chem. Phys. 87, 697–705 (1987).

56. Qiu, J., Mongcopa, K. I., Han, R., López-Barrón, C. R., Robertson, M. L. & Krishnamoorti, R. Thermodynamic Interactions in a Model Polydiene/Polyolefin Blend Based on 1,2-Polybutadiene. Macromolecules 51, 3107–3115 (2018).